Monthly Notices of the ROYAL ASTRONOMICAL SOCIETY

MNRAS **500,** 2496–2502 (2021) doi:10.1093/mnras/staa3392
Advance Access publication 2020 November 4

Radiative association for the formation of MgO

Tianrui Bai,[1] Zhi Qin[2,3]★ and Linhua Liu[1,2]★

[1]*School of Energy and Power Engineering, Shandong University, Jinan, Shandong 250061, China*
[2]*Optics and Thermal Radiation Research Center, Shandong University, Qingdao, Shandong 266237, China*
[3]*School of Information Science and Engineering, Shandong University, Qingdao, Shandong 266237, China*

Accepted 2020 October 17. Received 2020 October 17; in original form 2020 September 2

ABSTRACT

The radiative association process for the formation of magnesium oxide (MgO) may be of great importance due to its frequent occurrence in the low-density and dust-poor astrochemical environments. In this work, the cross-sections and rate coefficients for the $A^1\Pi \rightarrow X^1\Sigma^+$, $X^1\Sigma^+ \rightarrow A^1\Pi$, $D^1\Delta \rightarrow A^1\Pi$, $a^3\Pi \rightarrow e^3\Sigma^-$, $X^1\Sigma^+ \rightarrow X^1\Sigma^+$, and $A^1\Pi \rightarrow A^1\Pi$ radiative association processes of forming MgO are theoretically estimated. The cross-sections for the transitions between the different states are obtained by using the semiclassical method for direct contributions and the Breit–Wigner theory as a complement for resonance contributions. For the transitions between the same states, the quantum mechanical method is used. The rate coefficients are then obtained from the cross-sections for the temperatures in the range of 10–10 000 K and the results are found to vary from 4.69×10^{-16} to 6.27×10^{-14} cm^3 s^{-1}. For temperatures lower than around 693 K, the rate coefficients for the $A^1\Pi \rightarrow X^1\Sigma^+$ process are dominant, which indicates this process is the most efficient way of producing MgO at low temperatures. However, the rate coefficients for the $D^1\Delta \rightarrow A^1\Pi$ process go through a rapid increase with increasing temperature and become dominant at higher temperatures. For other processes, their rate coefficients are several orders of magnitude lower than those for the two processes mentioned above. The results can be used to further investigate the formation and evolution of MgO in low density and hot gas close to the photosphere of evolved oxygen-rich stars.

Key words: astrochemistry – molecular processes – opacity – radiation mechanisms: general – stars: low-mass – ISM: molecules.

1 INTRODUCTION

Magnesium oxide (MgO) is of great interest in astrophysical observations because it is the major constituent of chondritic meteorites in the interstellar dust. A search for the strongest band of MgO has been performed in the lunar exosphere (Berezhnoy 2010; Berezhnoy et al. 2014). Besides, it has also been detected in the exosphere of Mercury by the *MESSENGER* spacecraft (Sarantos et al. 2011; Stockstill-Cahill et al. 2012), where the observed magnesium tail is hotter than can be expected. Killen et al. (2010) analysed it might be attributed to about 30 per cent of the magnesium vapour in molecular form (MgO) at the high temperature (>10 000 K). This behaviour is expected to be caused by the micrometeoroid impact (Cintala 1992; Morgan & Killen 1997; Killen et al. 2001). According to the quenching theory, chemical reactions led to the formation of metallic oxides (e.g. MgO and CaO) during the collisional phase of the cloud created by the micrometeoroid impact (Berezhnoy & Klumov 2008; Berezhnoy 2010). The formation of MgO may be very likely to occur through radiative association in the collision of Mg and O atoms

$$\mathrm{Mg} + \mathrm{O} \rightarrow \mathrm{MgO} + \mathrm{h}\nu. \quad (1)$$

Magnesium, the most abundant cosmic metal, is believed to be formed as the results of the fusion of helium with neon in large stars and the addition of three helium nuclei to one carbon in supernovae. Besides, the atomic oxygen is also quite prevalent because it is the third most abundant element in the Universe. Therefore, the formation of an ionic bond between oxygen and magnesium (Mg–O) is inevitable due to both atoms' abundances and the large electrostatic attraction (Kloska & Fortenberry 2017).

The reaction in equation (1) is also one of many important processes that contributes to the molecule production in dust-poor regions of interstellar space where there are few competing three-body collisions (Tielens 2005). In fact, the density of an interstellar environment is often about 10^{-15} times than that of our atmosphere (Babb & Kirby 1998). Therefore, this process may be viable and important in the low-density and dust-poor astrochemical environments due to the applicability of two-body kinetics (Tabone et al. 2020).

The radiative association process for the formation of MgO is also believed to play a decisive role in initiating the dust formation process in oxygen-rich environments, because the Mg–O stretching vibrational band appears close to the Si–O deformation band and can easily merge with that to form the silicate (Rietmeijer et al. 2002; Schlemmer et al. 2014). Therefore, the rate coefficients of radiative association are required to model the chemical evolution of the dust formation in the interstellar space. However, due to the low rate coefficients of radiative association, only certain ionic systems are possible to be measured experimentally (Gerlich & Horning 1992). Hence, modelling of the interstellar environment about the chemical reaction (1) has to rely on the theoretical calculations (Gustafsson & Nyman 2014; Ostrom et al. 2016). Up to now, the radiative

★ E-mail: z.qin@sdu.edu.cn (ZQ); liulinhua@sdu.edu.cn (LL)

association process for the formation of MgO, which is important in astrophysics, has not been investigated theoretically. Thus, it is urgent to obtain an accurate and comprehensive theoretical investigation on the radiative association process for the formation of MgO.

The rate coefficients of radiative association have been investigated theoretically for a number of neutral and ionic systems. For example, the radiation association processes of diatomic molecules, such as CN, CO, CF^+, CO^+, C_2, TiO, SiS, SiO, etc., have been calculated in the past few years (Andreazza & Marinho 2007; Andreazza et al. 2012; Ostrom et al. 2016; Babb et al. 2019b; Gustafsson & Forrey 2019; Zámečníková et al. 2020). Andreazza et al. (G2, 2012) mainly calculated rate coefficients for the formation of the numerous diatomic molecules by the semiclassical (SC) method. For the researches of Babb et al. (2019a, b) and Forrey et al. (2020), they focused on the quantum mechanical (QM) theory in the local thermodynamic equilibrium (LTE) and non-LTE (NLTE). Gustafsson and Forrey (2019) concentrated on the different theoretical mechanisms for radiative association processes, which mainly included the QM, SC, optical potential (OP), and Breit–Wigner (BW) theories. Through the comparison, some findings about the QM theory were obtained by Gustafsson et al. First, they found that the QM method in the LTE might be cumbersome even for a diatomic system due to the narrow resonances at high energies. Secondly, compared with the BW theory, the QM method also might overestimate the heights of the resonances and the peak and shape of the resonances in the cross-sections were incorrect. Thirdly, the transitions from the quasi-bound to quasi-bound states were not included in the QM method (Bennett et al. 2003; Szabo & Gustafsson 2018). However, the BW theory could provide a complete description of the resonances in the whole energy range. Hence, in this work the BW theory is used to calculate the cross-sections and rate coefficients as the resonance contribution for the transitions between the different electronic states, and the SC method is used as the direct contribution to complement the BW theory. For the transitions between the same electronic states, the cross-sections and rate coefficients are calculated by the QM method.

We are chiefly concerned with the rate coefficients of the reaction (1) for the conditions of the LTE through the following transitions:

$$A^1\Pi\,[Mg(^1S) + O(^1D)] \rightarrow MgO\,(X^1\Sigma^+) + h\nu(A \rightarrow X) \quad (2)$$

$$X^1\Sigma^+\,[Mg(^1S) + O(^1D)] \rightarrow MgO\,(A^1\Pi) + h\nu(X \rightarrow A) \quad (3)$$

$$D^1\Delta\,[Mg(^1S) + O(^1D)] \rightarrow MgO\,(A^1\Pi) + h\nu(D \rightarrow A) \quad (4)$$

$$a^3\Pi\,[Mg(^1S) + O(^3P)] \rightarrow MgO(e^3\Sigma^-) + h\nu(a \rightarrow e) \quad (5)$$

$$X^1\Sigma^+\,[Mg(^1S) + O(^1D)] \rightarrow MgO\,(X^1\Sigma^+) + h\nu(X \rightarrow X) \quad (6)$$

$$A^1\Pi\,[Mg(^1S) + O(^1D)] \rightarrow MgO(A^1\Pi) + h\nu(A \rightarrow A) \quad (7)$$

The accurate potential energy curves (PECs) of the five electronic states involved in the above radiative association processes have been investigated by the state-of-the-art *ab initio* methodology in our previous work, but the transition dipole moments (TDMs) between these electronic states have not been computed (Bai et al. 2020). Thus, the TDMs for electronic transition systems considered here are calculated in the first step. Then, according to the calculated PECs and TDMs, the cross-sections are obtained using the SC method, BW theory, and QM method. Finally, the rate coefficients are computed based on the cross-sections

2 METHODS

This section presents the approach to the calculation of rate coefficients for the formation of MgO. The computational details on the PECs and TDMs are described to obtain the cross-sections. Thus, the further calculations based on the cross-sections can be carried out to get the rate coefficients.

2.1 Potential energy and transition moment curves

The accurate PECs of MgO have been investigated and more details on the *ab initio* calculations can refer to our previous work (Bai et al. 2020). The PECs of the $X^1\Sigma^+$, $A^1\Pi$, $D^1\Delta$, $a^3\Pi$, and $e^3\Sigma^-$ states are calculated at the icMRCI/aug-cc- pCV5Z-DK level of theory as implemented in MOLPRO 2015 software package (Werner et al. 2015). In this work, the dipole-allowed TDMs between these electronic states are calculated using the same theory as the calculated PECs.

For the calculation of rate coefficients, the PECs and TDMs are needed over the short and long range of internuclear distances R. In this work, the PECs are extrapolated toward zero by the following function at the short range:

$$V(R) = A\exp(-BR) + C. \quad (8)$$

For the large distances ($R > 10$ Å), the extrapolation method called the reciprocal-power reproducing kernel Hilbert space (RP-RKHS) is used with the leading term C_2/R^2 (Douglas & Kroll 1974; Hess 1986; Wolf et al. 2002). A cubic spline is used to interpolate the *ab initio* points of the PECs. For the TDMs, the same methods of extrapolation and interpolation as the PECs are used.

2.2 Rate coefficients

The total rate coefficients α_{tot} for the formation of a bound molecule can be expressed as

$$\alpha_{tot}(T) = \sum_{\Lambda\rightarrow\Lambda'} \alpha_{\Lambda\rightarrow\Lambda'}(T), \quad (9)$$

where $\alpha_{\Lambda\rightarrow\Lambda'}(T)$ are the rate coefficients for the specific electronic transition process, $\Lambda \rightarrow \Lambda'$, which can be calculated by averaging cross-sections over a Maxwellian velocity distribution and given by

$$\alpha_{\Lambda\rightarrow\Lambda'}(T) = \sqrt{\frac{8}{\pi\mu(k_BT)^3}}\int_0^\infty E\sigma_{\Lambda\rightarrow\Lambda'}(E)e^{(-E/k_BT)}dE, \quad (10)$$

where μ is the reduced mass, and $\sigma_{\Lambda\rightarrow\Lambda'}(E)$ are the cross-sections for the process of interest, as a function of the collision energy E. The cross-sections of the radiative association may be consisted of a direct and an indirect contribution, where the direct contribution can be obtained by the SC calculation and the BW theory can be used to calculate the indirect (resonance) contribution (Nyman et al. 2015).

2.3 Semiclassical method

The SC method is deduced from the SC limit of the OP method. The cross-sections for the $\Lambda \rightarrow \Lambda'$ transition can be expressed as (Bates 1951; Burhop & Marriott 1956)

$$\sigma_{\Lambda\rightarrow\Lambda'}(E) = 4\pi\sqrt{\frac{\mu}{2E}}f_\Lambda\int_0^\infty bdb\int_{R_c}^\infty \frac{A^{Eb}_{\Lambda\rightarrow\Lambda'}(R)}{\sqrt{1-\frac{V_\lambda(R)}{E}-\frac{b^2}{R^2}}}dR, \quad (11)$$

where b is the impact parameter. R_c is the outer turning point on the effective potential $V_\Lambda + Eb^2/R^2$, which can be found out using a bisection method. f_Λ is the probability of approach in the initial

electronic state characterized by Λ, which ignores the hyperfine couplings at the low energies. For the formation of a diatomic MgO from the atoms Mg and O, the factor f_Λ is given by

$$f_\Lambda = \frac{(2S+1)(2-\delta_{0,\Lambda})}{(2L_{\rm Mg}+1)(2S_{\rm Mg}+1)(2L_{\rm O}+1)(2S_{\rm O}+1)}, \quad (12)$$

where δ is the Kronecker delta. S is the spin quantum number of the electronic state Λ. $L_{\rm Mg}$, $S_{\rm Mg}$, $L_{\rm O}$, and $S_{\rm O}$ are the electronic orbital angular momentum number and spin quantum number of the atoms Mg and O, respectively. Therefore, the values of f_Λ are 2/5 for the $A^1\Pi$ and $D^1\Delta$ states and 1/3 for the $e^3\Sigma^-$ state. $A_{\Lambda\to\Lambda'}$ is the transition rate for spontaneous emission from an initial electronic state Λ to a final electronic state Λ' and

$$A_{\Lambda\to\Lambda'}(R) = \frac{64}{3}\frac{\pi^4}{(4\pi\varepsilon_0)h\lambda^3_{\Lambda\to\Lambda'}(R)}\left(\frac{2-\delta_{0,\Lambda+\Lambda'}}{2-\delta_{0,\Lambda}}\right)D^2_{\Lambda\Lambda'}(R), \quad (13)$$

where $D_{\Lambda\Lambda'}$ is the TDM between two arbitrary electronic states with the same spin quantum number. $\lambda_{\Lambda\to\Lambda'}(R)$ is the wavelength of the emitted photon, which is computed by

$$\frac{1}{\lambda_{\Lambda\to\Lambda'}(R)} = \max\left(0, \frac{V_\Lambda(R)-V_{\Lambda'}(R)}{hc}\right). \quad (14)$$

For the formation of a bonded molecule, the restricted transition rate should be applied

$$A^{Eb}_{\Lambda\to\Lambda'}(R) = A_{\Lambda\to\Lambda'}(R) \quad (15)$$

if $E < V_\Lambda(R) - V_{\Lambda'}(R)$ and $V_{\Lambda'}(R) + \frac{Eb^2}{R^2} < V_{\Lambda'}(R\to\infty)$; otherwise: $A^{Eb}_{\Lambda\to\Lambda'}(R) = 0$.

2.4 Breit–Wigner theory

The indirect contribution to the cross-sections of the radiative association is primarily tunnelling mediated, which arises from the resonances. The resonances arise not only from tunnelling through the barrier in the effective potential but also from 'overbarrier' resonances that can occur just over the barrier in the effective potential (Nyman et al. 2015). However, the SC method can only give the direct contribution to the cross-sections and cannot take resonances into account at all. Therefore, the BW theory is proposed and works as a complement to the SC method to compute the indirect contribution (Breit & Wigner 1936; Bain & Bardsley 1972).

Based on the BW theory, the resonance contribution to the cross-sections can be written as

$$\sigma^{\rm res}_{\Lambda\to\Lambda'}(E) = \frac{\pi\hbar^2}{2\mu E}f_\Lambda\sum_{\upsilon J}(2J+1)\frac{\Gamma^{\rm tun}_{\upsilon J\Lambda}\Gamma^{\rm rad}_{\upsilon J\Lambda}}{(E-E_{\upsilon J\Lambda})^2+\frac{\Gamma^2_{\upsilon J\Lambda\to\Lambda'}}{4}}. \quad (16)$$

The corresponding rate coefficients are given by

$$\alpha^{\rm res}_{\Lambda\to\Lambda'}(T) = \hbar^2\left(\frac{2\pi}{\mu k_{\rm B}T}\right)^{3/2}f_\Lambda\sum_{\upsilon,J}(2J+1) \times {\rm e}^{-E_{\upsilon J\Lambda}/k_BT}\frac{\Gamma^{\rm tun}_{\upsilon J\Lambda}\Gamma^{\rm rad}_{\upsilon J\Lambda\to\Lambda'}}{\Gamma_{\upsilon J\Lambda\to\Lambda'}}, \quad (17)$$

where $E_{\upsilon J\Lambda}$ is the energy of a quasi-bound state with quantum numbers Λ, υ, J, and is also the position of the resonances. $\Gamma^{\rm tun}_{\upsilon J\Lambda}$ is the tunnelling width. $\Gamma^{\rm rad}_{\upsilon J\Lambda\to\Lambda'}$ is the sum over the widths due to radiative decay from the initial state to any of the bound and lower lying quasi-bound states, $\Gamma^{\rm rad}_{\upsilon J\Lambda\to\Lambda'} = \hbar\sum_{\upsilon' J'}A_{\upsilon J\Lambda\to\upsilon' J'\Lambda'}$. The tunnelling width $\Gamma^{\rm tun}_{\upsilon J\Lambda}$ and transition rate for spontaneous emission $A_{\upsilon J\Lambda\to\upsilon' J'\Lambda'}$ are computed with the LEVEL 8.0 program package (Le Roy 2017). $\Gamma_{\upsilon J\Lambda\to\Lambda'}$ is the total width due to the decay either by tunnelling back through the potential barrier to separated atoms or by emitting a photon, $\Gamma_{\upsilon J\Lambda\to\Lambda'} = \Gamma^{\rm tun}_{\upsilon J\Lambda} + \Gamma^{\rm rad}_{\upsilon J\Lambda\to\Lambda'}$.

2.5 Quantum mechanical method

The QM method is based on the SC theory of light–matter interactions and thermodynamic relations for the Einstein coefficient describing the spontaneous emission of a photon (Golubev et al. 2013; Nyman et al. 2015). The cross-sections can be given by

$$\sigma_{\Lambda\to\Lambda'} = \sum_{J;\upsilon',J'}\frac{1}{4\pi\varepsilon_0}\frac{64}{3}\frac{\pi^5}{k^2}\left(\frac{\upsilon}{c}\right)f_\Lambda S_{\Lambda,J\to\Lambda',J'}|M_{\Lambda,E,J;\Lambda',\upsilon',J'}|^2, \quad (18)$$

where ε_0 is the vacuum permittivity, $k_2 = 2\mu E/\hbar^2$ and $S_{\Lambda J\to\Lambda' J'}$ is the H"onl-London factor (Hansson & Watson 2005; Watson 2008). $M_{\Lambda,E,J;\Lambda',\upsilon',J'}$ is the electric dipole transition moment function and can be expressed by

$$M_{\Lambda,E,J;\Lambda',\upsilon',J'} = \langle\chi_{E,J}(R)|D(R)\psi_{\upsilon',J'}(R)\rangle, \quad (19)$$

where $D(R)$ is the TDM from *ab initio*, $\chi_{E,J}(R)$ is the normalized wavefunction of the initial continuum state, and $\psi_{\upsilon',J'}(R)$ is the bound wavefunction by solving the radial Schrodinger equation. The renormalized Numerov method is used to obtain the continuum and bound wave functions (Johnson 1977, 1978).

3 RESULTS AND DISCUSSION

3.1 Potential energy and transition moment curves

In this work, five electronic states, including the $X^1\Sigma^+$, $A^1\Pi$, $D^1\Delta$, $a^3\Pi$, and $e^3\Sigma^-$ states, are calculated and investigated theoretically. These states correlate to the two lowest dissociation asymptotes $Mg(^1S) + O(^3P)$ and $Mg(^1S) + O(^1D)$. Fig. 1 shows the PECs of the five electronic states and the TDMs between these states versus the internuclear distances. The PECs have been computed in our previous work and the spectroscopic parameters are in good agreement with the experimental values (Bai et al. 2020). The $X^1\Sigma^+$ state is crossed by the $a^3\Pi$ and $A^1\Pi$ states at around 2.0 and 2.1 Å, respectively. It is beneficial to the interactions between these states through spin–orbit and rotational and vibronic couplings. Thus, the $X^1\Sigma^+$, $A^1\Pi$, and $a^3\Pi$ states are of interest in astrophysics and also the focal point in our work. Besides, the TDMs are also calculated as shown in Fig. 1(c). Our TDMs are also consistent with the earlier theoretical ones (Maatouk et al. 2010; Bauschlicher Jr & Schwenke 2017).

3.2 Cross-sections

The cross-sections for the radiative association processes (2)–(7) for the formation of MgO are calculated by the SC method, BW theory, and QM method. The calculated SC + BW, pure SC, and QM cross-sections are displayed in Fig. 2, where the SC + BW cross-sections are the sum of the direct contribution by the SC method and the resonance contribution obtained by the BW formula.

3.2.1 The $A^1\Pi \to X^1\Sigma^+$ *process*

The cross-sections for the $A^1\Pi \to X^1\Sigma^+$ radiative association process are displayed in Fig. 2(a). The SC cross-section curve is smooth but the BW cross-section curve exhibits many peaks

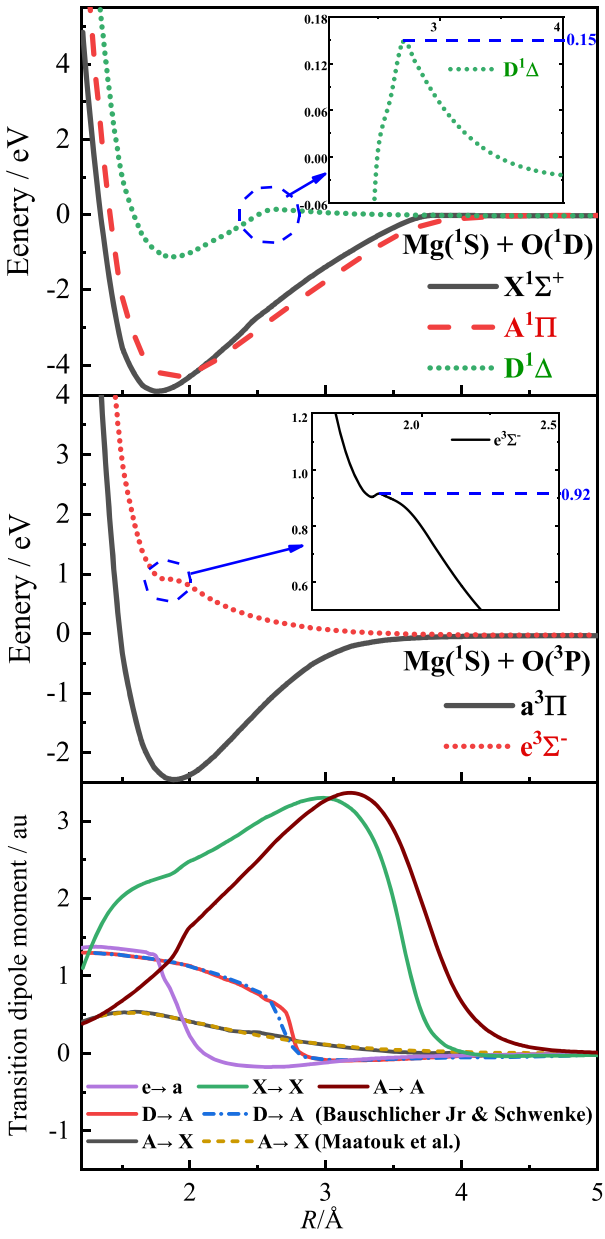

Figure 1. *Ab initio* points calculated at the icMRCI/aug-cc- pCV5Z-DK level of theory. (a) The PECs of the $X^1\Sigma^+$, $A^1\Pi$, and $D^1\Delta$ states. (b) The PECs of the $a^3\Pi$ and $e^3\Sigma^-$ states. (c) The TDMs for the $A^1\Pi \rightarrow X^1\Sigma^+$ ($X^1\Sigma^+ \rightarrow A^1\Pi$) transition compared with those from Maatouk et al. (2010), the $D^1\Delta \rightarrow A^1\Pi$ transition compared with those from Bauschlicher Jr & Schwenke (2017), and the $e^3\Sigma^- \rightarrow a^3\Pi$, $X^1\Sigma^+ \rightarrow X^1\Sigma^+$, and $A^1\Pi \rightarrow A^1\Pi$ transitions.

that come from the resonances. For energies less than 0.2 meV, the partial cross-sections remain almost constant as the collision energies increase. However, they decrease monotonically as the collision energies are larger than 0.2meV. Compared with other studied radiative association processes, the cross-sections for the $A^1\Pi \rightarrow X^1\Sigma^+$ process are the largest until the collision energy goes up to about 0.15 eV. This is due to a barrier on the $D^1\Delta$ electronic state, as shown in Fig. 1(a). In addition, the $A^1\Pi \rightarrow X^1\Sigma^+$ process has more resonances than other radiative association processes due to the deeper potential well of the $A^1\Pi$ state.

3.2.2 *The* $X^1\Sigma^+ \rightarrow A^1\Pi$ *process*

Fig. 2(b) shows the cross-sections for the $X^1\Sigma^+ \rightarrow A^1\Pi$ process, which have the same tendency as those for the $A^1\Pi \rightarrow X^1\Sigma^+$ process but are smaller over the range of collision energies. For high collision energies (>0.395 eV), the SC cross-sections approach zero very quickly, because non-Franck–Condon transitions are not accounted for the SC theory (Franck & Dymond 1926; Condon 1928). Meanwhile, the $X^1\Sigma^+ \rightarrow A^1\Pi$ process has few resonances, because the cross-sections calculated by the BW theory are much smaller than those by the SC method.

3.2.3 *The* $D^1\Delta \rightarrow A^1\Pi$ *process*

As shown in Fig. 2(c), the $D^1\Delta \rightarrow A^1\Pi$ cross-sections are smaller than those for the $A^1\Pi \rightarrow X^1\Sigma^+$ process for energies less than 0.15 eV. However, as the collision energies increase, the cross-sections go up rapidly from 1.53×10^{-7} to 4×10^{-5} a_0^2 and this process thus becomes dominant. It is due to a 0.15eV barrier at 2.7 Å on the $D^1\Delta$ electronic state as mentioned above. This behaviour can be generally found in other similar system, such as the $1^1\Pi \rightarrow X^1\Sigma^+$ system and the $1^1\Pi \rightarrow a^3\Pi$ system of CF^+ (Ostrom et al. 2016). For high collision energies (>3.23 eV), the SC cross-sections approach zero very quickly because of non-Franck–Condon transitions.

3.2.4 *The* $e^3\Sigma^- \rightarrow a^3\Pi$ *process*

Fig. 2(d) shows the cross-sections for the $e^3\Sigma^- \rightarrow a^3\Pi$ process. Through comparison and observation, we can conclude several findings. First, the cross-sections for this process are smaller than those for the above processes and decrease rapidly with the decreasing collision energy because of the almost repulsive potential of the $e^3\Sigma^-$ state (Kathir et al. 2017). Secondly, the cross-sections increase rapidly at the collision energy of 0.92 eV because of a small potential barrier. This behaviour corresponds to the fact that the $e^3\Sigma^-$ potential exhibits a 0.92 eV barrier at $R = 1.84$ Å, as shown in Fig. 1(d). Thirdly, the BW cross-sections show few resonances at low energies, this is because the almost repulsive potential of the $e^3\Sigma^-$ state can only support few quasi-bound states. Finally, the SC cross-sections could not be calculated as the collision energies are higher than 3.36 eV due to the Franck–Condon principle.

3.2.5 *The* $X^1\Sigma^+ \rightarrow X^1\Sigma^+$ *and* $A^1\Pi \rightarrow A^1\Pi$ *processes*

The cross-sections for the $X^1\Sigma^+ \rightarrow X^1\Sigma^+$ and $A^1\Pi \rightarrow A^1\Pi$ processes are displayed in Fig. 2(e), which are obtained by the QM method. Due to the similar PECs and TDMs of the $X^1\Sigma^+$ and $A^1\Pi$ states, the cross-sections of these two processes are also similar. As the collision energies increase, the cross-sections change slowly and the baseline approaching on the $X^1\Sigma^+$ and $A^1\Pi$ curves is nearly constant with respect to the collision energy. The similar behaviour can be seen from other processes, such as the $X^1\Sigma^+ \rightarrow X^1\Sigma^+$ process of CO (Franz et al. 2011).

3.3 Rate coefficients

The rate coefficients for the formation of MgO through the studied six processes are calculated for temperatures in the range of 10–10 000 K (as shown in Fig. 3), which are the sum of the direct contribution from the SC method and the resonance contribution obtained by the BW theory. The magnitude of the rate coefficients is similar to that

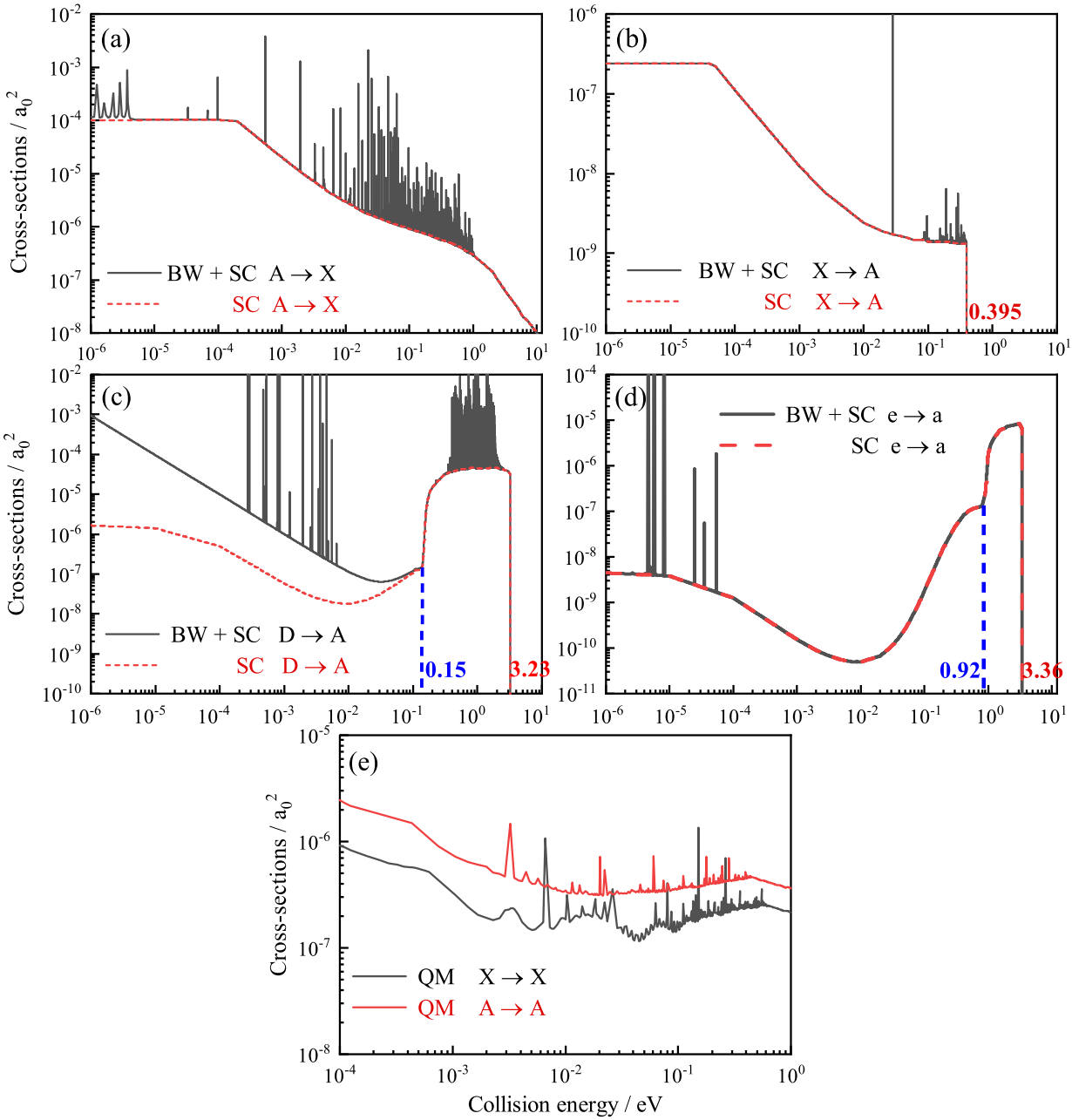

Figure 2. Cross-sections for the (a) $A^1\Pi \rightarrow X^1\Sigma^+$, (b) $X^1\Sigma^+ \rightarrow A^1\Pi$, (c) $D^1\Delta \rightarrow A^1\Pi$, and (d) $e^3\Sigma^- \rightarrow a^3\Pi$ transition processes calculated by the SC method and BW theory and the (e) $X^1\Sigma^+ \rightarrow X^1\Sigma^+$ and $A^1\Pi \rightarrow A^1\Pi$ transition processes by the QM method.

of the formation of other diatomic molecules (Andreazza & Marinho 2007; Cairnie et al. 2017; Zámečníková et al. 2020). As expected from the cross-sections, the $A^1\Pi \rightarrow X^1\Sigma^+$ process is dominant for temperatures lower than around 693 K. However, the $D^1\Delta \rightarrow A^1\Pi$ process undergoes a rapid increase with the increasing temperature and dominates at higher temperatures. For the $X^1\Sigma^+ \rightarrow A^1\Pi$, $X^1\Sigma^+ \rightarrow X^1\Sigma^+$, $A^1\Pi \rightarrow A^1\Pi$, and $e^3\Sigma^- \rightarrow a^3\Pi$ radiative association processes, the rate coefficients are several orders of magnitude lower than those for the $A^1\Pi \rightarrow X^1\Sigma^+$ and $D^1\Delta \rightarrow A^1\Pi$ processes, where the rate coefficients of the $e^3\Sigma^- \rightarrow a^3\Pi$ process increase monotonically as the temperature increases above 100 K because the PEC of the $e^3\Sigma^-$ state is almost completely repulsive. The similar behaviour can be seen from the work carried out by Gustafsson et al. (2014). The total rate coefficients for the formation of MgO are the sum of rate coefficients for all studied processes in this work and can be approximated using the three-parameter Kooij function (within 4 per cent), which is expressed as

$$k(T) = A\left(\frac{T}{300}\right)^{\alpha} e^{-\beta/T}, \tag{20}$$

where A, α, and β are fitting parameters. Due to a complex structure with multiple inflexion points on the temperature dependence of the rate coefficients, the rate coefficient curves are divided into seven temperature ranges to fit. The fitting parameters are summarized in Table 1.

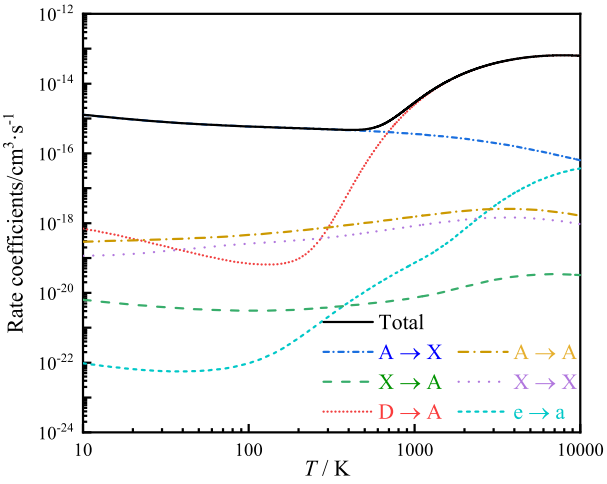

Figure 3. Radiative association rates (cm^3 s^{-1}) for the formation of MgO through the processes (2)–(7).

Table 1. Fit parameters according to Kooij function (equation 20) for the total rate coefficients.

T (K)	A (cm^3 s^{-1})	α	β
10–40	5.0943×10^{-16}	−0.4073	2.0976
40–460	5.0881×10^{-16}	−0.1793	0.1709
460–5200	6.0276×10^{-15}	1.2271	4.7817
5200–7200	4.1786×10^{-14}	0.2578	1.6307
7200–7800	5.9655×10^{-14}	0.0493	0.3384
7800–8000	6.6094×10^{-14}	−0.0133	−0.0966
8000–10 000	8.0820×10^{-14}	0.1409	−1.0554

4 CONCLUSIONS

In this work, the rate coefficients for the formation of MgO by radiative association mechanism have been studied theoretically. The accurate PECs of the $X^1\Sigma^+$, $A^1\Pi$, $D^1\Delta$, $a^3\Pi$, and $e^3\Sigma^-$ states and the TDMs between these electronic states are obtained by the state-of-the-art *ab initio* methodology. Thereafter, the cross-sections for the $A^1\Pi \rightarrow X^1\Sigma^+$, $X^1\Sigma^+ \rightarrow A^1\Pi$, $D^1\Delta \rightarrow A^1\Pi$, and $e^3\Sigma^- \rightarrow a^3\Pi$ processes are calculated by the SC method and BW theory. For the $X^1\Sigma^+ \rightarrow X^1\Sigma^+$ and $A^1\Pi \rightarrow A^1\Pi$ processes, the QM method is used. Finally, the rate coefficients are calculated for the temperatures in the range of 10–10 000 K. The magnitude of the rate coefficients of forming MgO is similar to that of the formation of other diatomic molecules, and the total rate coefficients are of the order of $4.69 \times 10^{-16} - 6.27 \times 10^{-14}$ cm^3 s^{-1}.

The cross-sections for the $A^1\Pi \rightarrow X^1\Sigma^+$ process are dominant and larger than those for other processes up to a collision energy of about 0.15 eV. It is attributed to a barrier on the $D^1\Delta$ electronic state, leading to the rapidly increasing cross-sections for the $D^1\Delta \rightarrow A^1\Pi$ process from 1.53×10^{-7} to 4×10^{-5} a_0^2. Thus, the $D^1\Delta \rightarrow A^1\Pi$ process becomes dominant at high collision energies. However, the cross-sections for the $X^1\Sigma^+ \rightarrow A^1\Pi$, $X^1\Sigma^+ \rightarrow X^1\Sigma^+$, $A^1\Pi \rightarrow A^1\Pi$, and $e^3\Sigma^- \rightarrow a^3\Pi$ processes are smaller within the studied energy range.

As expected from the cross-sections, the rate coefficients calculated by the SC + BW approach have the similar changes. For example, for temperatures lower than around 693 K, the $A^1\Pi \rightarrow X^1\Sigma^+$ process is dominant. As the temperatures increase, the $D^1\Delta \rightarrow A^1\Pi$ process undergoes a rapid increase and becomes dominant. Corresponding to the cross-sections, the calculated rate coefficients for the $X^1\Sigma^+ \rightarrow A^1\Pi$, $X^1\Sigma^+ \rightarrow X^1\Sigma^+$, $A^1\Pi \rightarrow A^1\Pi$, and $e^3\Sigma^- \rightarrow a^3\Pi$ processes are several orders of magnitude lower than those for other processes.

The rate coefficients calculated in this work can be used to the community of astrochemists who investigate the chemical evolution of dust formation in the interstellar space. Meanwhile, the rate coefficients for radiative association can also be further used to estimate three-body recombination rates at the critical density where the collisional and radiative rates are the same (Cairnie et al. 2017).

ACKNOWLEDGEMENTS

This work is sponsored by the National Natural Science Foundation of China under Grant no. 51336002, 51421063. We acknowledge Dr Martina Zámečníková's kind and helpful guidances for understanding the Breit-Wigner theory.

DATA AVAILABILITY STATEMENT

The data underlying this article are available in the article and in its online supplementary material. These include the rate coefficients of the A-A, A-X, D-A, e-a, X-A, and X-X transition processes, as well as the total rate coefficients of these processes (corresponding to Fig. 3).

REFERENCES

Andreazza C. M., De Almeida A., Vichietti R. M., Ceccatto D. T., 2012, MNRAS, 427, 833
Andreazza C. M., Marinho E. P., 2007, MNRAS, 380, 365
Babb J. F., Kirby K. P., 1998, in Hartquist T. W. D. A. W., ed., Molecule Formation in Dust-poor Environments. Clarendon, Oxford, p. 11
Babb J. F., Smyth R. T., Mclaughlin B. M., 2019a, ApJ, 876, 38
Babb J. F., Smyth R. T., Mclaughlin B. M., 2019b, ApJ, 884, 155
Bain R. A., Bardsley J. N., 1972, Phys. Rev. B, 5, 277
Bai T., Qin Z., Liu L., 2020, J. Quant. Spectrosc. Radiat. Transfer, 251, 107086
Bates D. R., 1951, MNRAS, 111, 303
Bauschlicher C. W., Jr, Schwenke D. W., 2017, Chem. Phys. Lett., 683, 62
Bennett O. J., Dickinson A. S., Leininger T., Gadéa F. X., 2003, MNRAS, 341, 361
Berezhnoy A. A., 2010, Adv. Space Res., 45, 70
Berezhnoy A. A., Klumov B. A., 2008, Icarus, 195, 511
Berezhnoy A. A. et al., 2014, Planet. Space Sci., 96, 90
Breit G., Wigner E., 1936, Phys. Rev., 49, 519
Burhop E. H.S., Marriott R., 1956, Proc. Phys. Soc., 69, 271
Cairnie M., Forrey R. C., Babb J. F., Stancil P. C., Mclaughlin B. M., 2017, MNRAS, 471, 2481
Cintala M. J., 1992, J.Geophys. Res., 97, 947
Condon E. U., 1928, Phys. Rev., 32, 858
Douglas M., Kroll N. M., 1974, Ann. Phys., 82, 89
Forrey R. C., Babb J. F., Courtney E. D.S., McArdle R. T., Stancil P. C., 2020, ApJ, 898, 86
Franck J., Dymond E. G., 1926, Trans. Faraday Soc., 21, 536
Franz J., , Gustafsson M., Nyman G., 2011, MNRAS, 414, 3547
Gerlich D., Horning S., 1992, Chem. Rev., 92, 1509
Golubev N. V., Bezrukov D. S., Gustafsson M., Nyman G., Antipov S. V., 2013, J. Phys. Chem. A, 117, 8184
Gustafsson M., Forrey R. C., 2019, J. Chem. Phys., 150, 224301
Gustafsson M., Monge-Palacios M., Nyman G., 2014, J. Chem. Phys., 140, 184301
Gustafsson M., Nyman G., 2014, J. Phys. Conf. Ser., 548, 012003
Hansson A., Watson J. K.G., 2005, J. Mol. Spectrosc., 223, 169
Hess B. A., 1986, Phys. Rev. A, 33, 3742

Johnson B. R., 1977, J. Chem. Phys., 67, 4086
Johnson B. R., 1978, J. Chem. Phys, 69, 4678
Kathir R. K., Nyman G., Gustafsson M., 2017, MNRAS, 470, 3068
Killen R. M., Potter A. E., Reiff P. H., Sarantos M., Jackson B. V., Hick P., Giles B., 2001, J. Geophys. Res., 106, 20509
Killen R. M., Potter A. E., Vervack R. J., Bradley E. T., Mcclintock W. E., Anderson C. M., Burger M. H., 2010, Icarus, 209, 75
Kloska K. A., Fortenberry R. C., 2017, MNRAS, 474, 2055
Le Roy R. J., 2017, J. Quant. Spectrosc. Radiat. Transfer, 186, 167
Maatouk A., Ben Houria A., Yazidi O., Jaidane N., Hochlaf M., 2010, J. Chem. Phys., 133, 144302
Morgan T. H., Killen R. M., 1997, Planet. Space Sci., 45, 81
Nyman G., Gustafsson M., Antipov S. V., 2015, Int. Rev. Phys. Chem., 34, 385
Ostrom J., Bezrukov D. S., Nyman G., Gustafsson M., 2016, J. Chem. Phys., 144, 044302
Rietmeijer F. J. M., Nuth J. A., Karner J. M., Hallenbeck S. L., 2002, Phys. Chem. Chem. Phys., 4, 546
Sarantos M., Killen R. M., Mcclintock W. E., Bradley E. T., Vervack R. J., Benna M., Slavin J. A., 2011, Planet. Space Sci., 59, 1992
Schlemmer S., Mutschke H., Giesen T., Jäger C., 2014, in Schlemmer S., Giesen T., Mutschke H., Jäger C., eds, Laboratory Astrochemistry: From Molecules through Nanoparticles to Grains. Wiley-VCH, Germany, p. 356
Stockstill-Cahill K. R., McCoy T. J., Nittler L. R., Weider S. Z., Hauck S. A., 2012, J. Geophys. Res., 117, E00L15
Szabo P., Gustafsson M., 2018, MNRAS, 483, 3574
Tabone B., Godard B., Des Forets G. P., Cabrit S., Van Dishoeck E. F., 2020, A&A, 3, 1
Tielens A. G. G. M., 2005, The Physics and Chemistry of the Interstellar Medium. Cambridge University Press, New York, p. 85
Watson J. K. G., 2008, J. Mol. Spectrosc., 252, 5
Werner H.-J. et al., MOLPRO, Version 2015.1, A Package of Ab Initio Programs, Available at: http://www.molpro.net
Wolf A., Reiher M., Hess B. A., 2002, J. Chem. Phys., 117, 9215
Zámečníková M., Gustafsson M., Nyman G., Soldán P., 2020, MNRAS, 492, 3794

SUPPORTING INFORMATION

Supplementary data are available at *MNRAS* online.

Supplemental material.zip

Please note: Oxford University Press is not responsible for the content or functionality of any supporting materials supplied by the authors. Any queries (other than missing material) should be directed to the corresponding author for the article.

This paper has been typeset from a TEX/LATEX file prepared by the author.